A Method of Tactile Resistive Sensor Array Calibration

Conference Paper *in* IFAC-PapersOnLine · June 2024

DOI: 10.1016/j.ifacol.2024.07.368

4 authors, including:

M. Husák
Brno University of Technology
14 PUBLICATIONS **24** CITATIONS
SEE PROFILE

Ondrej Mihálik
Brno University of Technology
27 PUBLICATIONS **39** CITATIONS
SEE PROFILE

Zdenek Bradac
Brno University of Technology
110 PUBLICATIONS **982** CITATIONS
SEE PROFILE

Available online at www.sciencedirect.com

ScienceDirect

IFAC PapersOnline CONFERENCE PAPER ARCHIVE

IFAC PapersOnLine 58-9 (2024) 37–42

A Method of Tactile Resistive Sensor Array Calibration

Michal Husák * **Ondrej Mihálik** * **Petr Dvorský** *
Zdeněk Bradáč **

* *Faculty of Electrical Engineering and Communication, Brno University of Technology, Brno, Czechia (e-mail: michal.husak@vut.cz).*
** *Central European Institute of Technology, Brno University of Technology, Brno, Czechia (e-mail: zdenek.bradac@ceitec.vutbr.cz).*

Abstract: Resistive sensor arrays (RSA) comprising of pressure-sensitive elements find broad use in pressure-sensing applications. However, sensor manufacturing inevitably yields a number of non-ideal properties. The gain, offset or non-linearities of an RSA's elements may vary between individual sensors (taxels). Hence a simple calibration procedure to suppress these effects is desirable. The paper presents a method of and apparatus for the calibration of a pressure-sensing RSA. A forward mathematical model for each sensor is obtained during the calibration phase. In subsequent online measurement, the inverse model is utilised to compensated for the non-uniformity in sensor gain and offset. This approach leads to an appreciable improvement in picture quality, which can be mathematically quantified using classification accuracy in our tactile anti-decubitus platform for human monitoring. Namely, in a four-class classification experiment involving a support vector machine, the classification error decreased from 11 % before calibration to 3.5 % after calibration. Owing to the calibration procedure, a classifier trained using a calibrated RSA can be deployed to another calibrated RSA, without further data collection.

Keywords: calibration, pressure, resistive sensor array, tactile platform, robustness

1. INTRODUCTION

Tactile resistive sensor arrays (RSA) find broad application in healthcare-related sensing applications, predominantly in wearable electronics developed by Meng et al. (2023); Zhang et al. (2023); Peters et al. (2023), or in pressure mapping mats and mattresses advanced by Wu et al. (2019); Nie et al. (2019); Hu et al. (2021).

If the low cost of manufactured sensors is imperative, materials with worse thermal or temporal stability must be resorted to. However dealing with non-ideal material properties requires that they are compensated for by a calibrated readout electronic or signal post-processing. Calibration methods for pressure RSA have been documented within many distinctive fields, such as thermal mapping, Bücher et al. (2022), collaborative robots, Pang et al. (2018), and wearable electronics Lin and Seet (2015).

We will narrow the discussion down to tactile RSAs. The most prominent researchers employ either black-box or analytical models. Bücher et al. (2022) and Müller et al. (2019) advance the former approach consisting in an artificial neural network (ANN). As an alternative with lighter computational complexity Halaj et al. (1998) and Gilanizadehdizaj et al. (2022) construct a polynomial model for each sensor of the RSA. In both cases the model parameters (the ANN's weights or polynomial coefficients) are learned from calibration data acquired using a calibration apparatus.

This paper explores calibration methodologies for the matrix tactile measurement platform and their application in assessing the temporal stability of the measurement device. The primary aim is to present a calibration process applicable to a force-sensing RSA and obtain its mathematical model, which can be used to provide scaled outputs in standard physical units. The force-sensing RSAs typically find application in posture classification or load mass determination. Therefore, in order to assess the benefit of calibration, we use classification accuracy as a definite measure of quality.

The paper is divided as follows. Section 2 describes the investigated pressure sensing mattress, calibration apparatus and collection of calibration data. Section 3 introduces the mathematical tools which evaluate the data. The forward and inverse sensor models are presented. The parameters of these models are presented in Section 4. Their time stability and correlation with temperature changes are also analysed.

2. MATERIAL AND METHODS

Pressure sensitive platforms are used in diverse fields and applications such as sleep cycle monitoring Byun et al. (2019), real time biometric body measurement's Nudzikova and Slanina (2016) and monitoring of elderly individuals residing in independent homes Xu et al. (2015). A similar platform was designed with the aim of posture classification, which plays a role in decubitus prevention,

10.1016/j.ifacol.2024.07.368

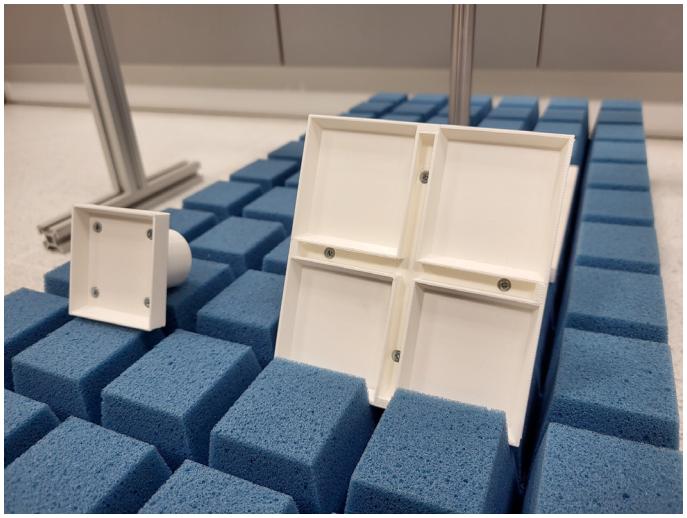

Fig. 1. Calibration taxel holder for one taxel (left) and calibration matrix holder dimension 2×2 (right).

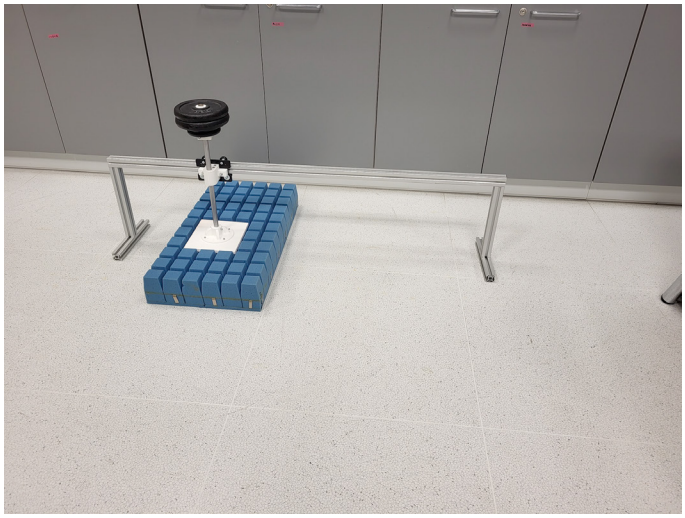

Fig. 2. Calibration platform with linear gearing for weight stability (demonstrated on one segment of the pressure bed).

and our first classification results were presented in previous works of Husák et al. (2021); Mihálik et al. (2022). Our platform consists of 30×11 piezoresistive pressure points, which is smaller than Liu et al. (2023). We focus on simplicity and cost-effectiveness, essential attributes for the integration of the device into domestic settings. The RSA consists of Velostat® piezoresistive elements, as commonly used in tactile applications, e.g. Dzedzickis et al. (2020). The pressure sensitive material is intricately embedded within the core of the foam mattress. The foam which covers individual sensors, shown in Figure 1, has been shaped so that it suppresses the effects of pressure propagation, also known as mechanical crosstalk. The inherent characteristics of the foam made of polyurethane material, coupled with the physical attributes of the pressure element, such as shape and material density, preclude application of substantial weights to individual sensors.

On one hand, Velostat® is an affordable material. On the other hand, it exhibits thermal and temporal instability reported e.g. by Dzedzickis et al. (2020). As mentioned in the introduction, such disadvantages require a form of compensation, which can be provided using mathematical models. If we adopt an efficient and computationally simple model, even a low-cost sensor can achieve the same performance as a more expensive one. In the low-cost sensor, the software is responsible for improving both the data readout quality from the matrix resistive sensor and the robustness of subsequent classification algorithms.

The assessment of temporal stability in the calibration models constitutes a pivotal aspect of our study. This parameter assumes a paramount role in influencing the robustness of the classification process, as even sophisticated classification methods, once learned, exhibit limited resilience to factors such as noise, bias, and data dropout.

Consequently, an innovative approach was necessitated, leading to the development of a calibration apparatus shown in Figure 2. As seen in the figure, a simple frame made of extruded aluminium is used to guide a carriage with linear guidance for the vertical calibration rod. The rod moves freely and therefore transfers the weight exerted by a known mass into a matrix that distributes the pressure force into a rectangular taxel or subset of taxels loaded simultaneously. The 3-D printed pressing matrices (visible in Figure 1) facilitate the modular loading of the sensing RSA: 3×3, 2×2, and even single-taxel. This apparatus is used to sequentially load taxels using a known force. The mass of the whole freely moving part was measured and added to the loading weights. Thus a calibration dataset is acquired and used to train a model of the RSA.

3. MATHEMATICAL MODEL

The task of calibration can be mathematically formulated as follows. Contemplate that a taxel located at position $[m, n]$ of the RSA has a static characteristic: The conductance of the taxel, G_{mn}, is a function of the pressure force, F_{mn}. In general, each taxel may have a different static response

$$G_{mn} = f_{mn}(F_{mn}),\ m = 1, 2, \ldots, M,\ n = 1, 2, \ldots, N. \quad (1)$$

Theoretically, we could sample each of the functions f_{mn} in sufficiently many points by applying defined forces and measuring corresponding conductance. However, if we cannot (or do not want to) indulge in the luxury of extensive data acquisition then we must make some simplifying assumptions about the functions f_{mn}.

In the case of Halaj et al. (1998), a concrete example is a simplifying assumption that the relations f_{mn} constitute linear functions

$$\begin{gathered} G_{mn} = a_{mn} F_{mn} + b_{mn}, \\ m = 1, 2, \ldots, M, \quad n = 1, 2, \ldots, N. \end{gathered} \quad (2)$$

The coefficients a_{mn} and b_{mn} may be sought using the least squares method. For instance, MATLAB affords the function `polyfit` which readily returns these coefficients. In other environments, one may make use of the well-known formulae

$$b = \frac{K \sum_{k=1}^{K} G(k)F(k) - \sum_{k=1}^{K} G(k) \sum_{k=1}^{K} F(k)}{K \sum_{k=1}^{K} F^2(k) - \left[\sum_{k=1}^{K} F(k)\right]^2} \quad (3a)$$

and

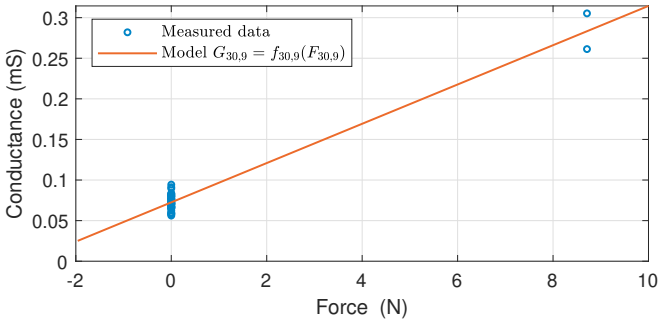

Fig. 3. Individual calibration measurements (blue) and corresponding linear taxel model (red). Taxel location $[m, n] = [30, 9]$.

$$a = \frac{\sum_{k=1}^{K} G(k) - b \sum_{k=1}^{K} F(k)}{K} \,. \tag{3b}$$

For the sake of simplicity, we left out the taxel indices $[m, n]$, but these equations are meant to be applied to each taxel separately. The K stands for the total number of measurements and the index k denotes the individual measurements (blue points in Figure 3).

During our calibration procedure, the weights were shifted into various positions $[m, n]$. The taxels without weight are not loaded by any force. Hence the measurements at point $F_{mn}(k) = 0$ N prevail. This is evident from Fig. 3. When the loading matrix of size 3×3 was used, the procedure yielded $K = 40$ different measurements: for each taxel, there are 38–39 measurements without load and 1–2 loaded measurements.

Once the models (2) are known, we employ the inverse function to compute the sought force F_{mn} using measured conductance G_{mn} according to

$$F_{mn} = \frac{G_{mn} - b_{mn}}{a_{mn}} \,, \quad m = 1, 2, \ldots, M, \quad n = 1, 2, \ldots, N. \tag{4}$$

This equation is evaluated online during the snapshot of the pressure sensing RSA.

The comparison of raw and calibrated pressure maps is shown in Fig. 4. The inverse model (4) significantly suppresses the non-uniformity caused during the manufacturing process and degradation during use; it yields a decided improvement in picture quality. Especially the random noise surrounding a person's body is much less pronounced.

4. RESULTS AND DISCUSSION

We focus in this section on the analysis of the calibration model parameters. The calibration process (3) yields $M \times N$ matrices $\mathbf{A}$ and $\mathbf{B}$, which contribute to the pressure result of each taxel. First, we will investigate whether the model parameters depend on the position or if they are random. Then we will discuss the thermal and temporal stability.

4.1 Visualization of the model's parameters

As mentioned above, this study investigates the deterioration of the mattress measuring platform. Evidently,

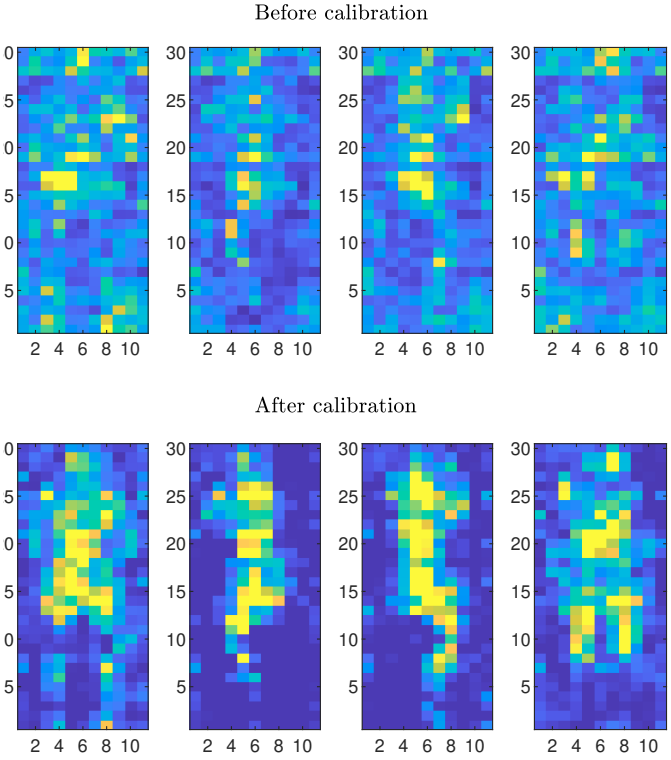

Fig. 4. Comparison of pressure maps before (top) and after calibration (bottom). The maps display subjects in lying in different position; left to right: supine, lateral right, lateral left, and prone.

the taxel sensitivity of the tactile platform exhibits a discernible U-shaped pattern rather than a purely random distribution, as shown in Figure 5. Namely, there is a distinctive decline in sensitivity within the centre of the RSA, which is the most stressed region. From this observation we infer that the taxel model experiences degradation under stress, necessitating periodic calibration, see Dzedzickis et al. (2020) for a detailed discussion.

The application of calibration proves effective in suppressing the influence of noise. Especially the noise originating from the unloaded surroundings of the figure outline was suppressed, see Figure 4. However, the presence of noise in the loaded areas becomes noticeable within the course of degradation. Therefore, a form of periodic calibration will be necessary.

4.2 Thermal stability of model parameters

Additionally, a source of measurement inaccuracy stems from the temperature dependence of taxel conductivity. It is imperative to address the temperature effect in accordance with

$$F_{mn} = \frac{G_{mn} - \beta_{mn}(\vartheta)}{\alpha_{mn}(\vartheta)} \,, \quad m = 1, 2, \ldots, M, \quad n = 1, 2, \ldots, N. \tag{5}$$

where ϑ denotes the temperature. The model parameters, denoted as functions $\alpha_{mn}(\vartheta)$ and $\beta_{mn}(\vartheta)$, are temperature dependent.

Figure 6 shows how the mean taxel gain a evolved over six months of operation. The original assumption was that

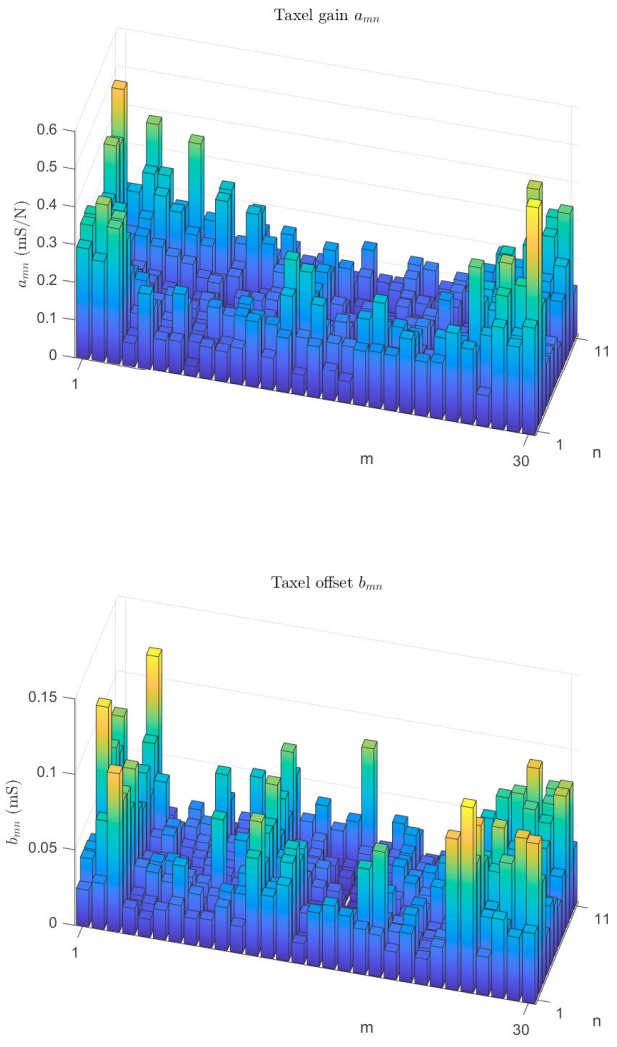

Fig. 5. Distribution of parameters, gain $a_{m,n}$ and offset $b_{m,n}$, across the matrix platform.

this plot might reveal a form of temporal trend. However, the reader may observe a significant correlation between a and the temperature ϑ. The Pearson correlation coefficient is –58.7 % (note that the temperature axis in Figure 6 is reversed). There, the temperature dependence should be compensated to achieve stability of measurements.

4.3 Force-to-picture transformation

The output of the measurement is a force matrix obtained through the relationship given in (4), which is used for weight calculation. However, it is not recommendable to use force directly as the input of machine learning methods that further analyze the pressure image; these methods typically assume a normalized input, as discussed in the standard machine learning textbooks Hastie et al. (2009). The data normalization is also useful for denoising by partially correcting the negative force values. As illustrated in Figure 4, it is also necessary to normalize the output image to a known range to ensure a perceptible colour

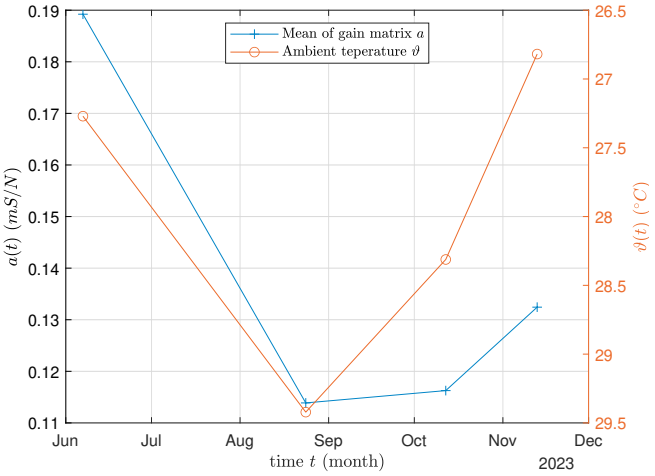

Fig. 6. Temporal variations of the mean taxel model and ambient temperature. The temperature axis is reversed to emphasize the significant correlation between temperature and taxel gain is observed.

scale. To normalize the output, we employed a piecewise linear function, as defined in Figure 7. The saturation provides a form of denoising by means of soft threshold, as commonly used in wavelet denoising, see Stéphane (2009); Hastie et al. (2009). The negative force is clearly attributed to measurement noise. Therefore, force below –2.4 N is assigned zero taxel value. Likewise, forces above 13.3 N are saturated to 100 % taxel value.

The knots of the linear spline were selected using our dataset comprising 1280 pressure images from individuals within the weight range of 60–110 kg, assuming various positions that are shown in Figure 4. The x-positions of the spline's knots are:

- minimum force in the dataset,
- 0 N force,
- 99th percentile of the dataset,
- maximum force in the dataset.

The spline's knots are shown in Figure 7.

The histogram of the calibrated force from the complete dataset is displayed in Figure 5 (top). These force values are mapped and squeezed into the interval 0–1 of taxel values using static transformation in Figure 7 which results in taxel histogram in Figure 8 (bottom). The application of histogram equalization ensures that the output signal retains all information while preserving extreme outliers. Due to the simplicity of the function, an inversion is also feasible, enabling the retrieval of pressure values.

4.4 Evaluation of calibration effect on classification

In order to quantify the importance of the presented calibration and transformation scheme we perform a posture classification experiment. Classification using the same but uncalibrated pressure sensing platform was previously reported by Husák et al. (2021); Mihálik et al. (2022); Mesárošová and Mihálik (2023). The posture of human subjects was classified into four distinct classes using ma-

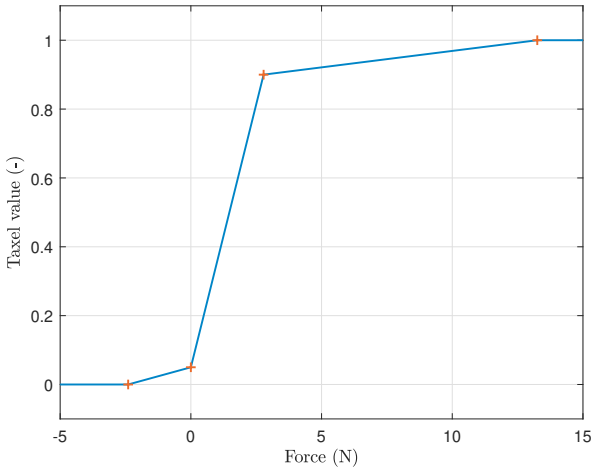

Fig. 7. Force to image transformation applied to each RSA's taxel. The knots are highlighted using red crosses.

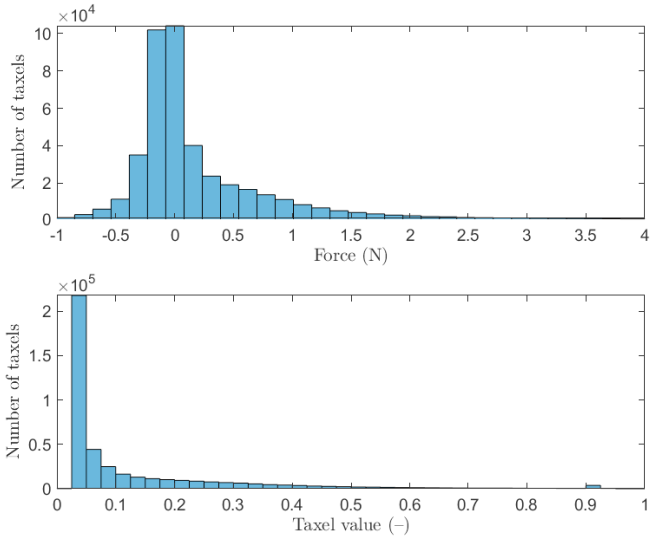

Fig. 8. Histogram of force distribution (top) and Scaled histogram of the pressure image taxel (bottom).

chine learning methods and their accuracy is expressed in terms of true positive rate (TPR).

All TPRs were obtained using a leave-one-person-out crossvalidation, which may be justified by the following considerations. Our classifiers are trained using human subjects who constitute a virtually nil fraction of the national population. In the final application, the probability that a different person is monitored approaches 100 %. To mimic this real-life scenario all pressure maps of the validation person are excluded from the training dataset. The classifier is trained using the remaining persons' pressure maps.

The validation is repeated in this manner for all participants. The final TPR is computed as the mean of TPRs of each validation person.

Likewise Mihálik et al. (2022), we select two popular classifiers: K nearest neighbours (KNN) and linear support vector machine (SVM), whose general descriptions are to be found in Hastie et al. (2009). The calibration has an appreciable positive effect on the classification accuracy expressed in Table 1. The classification error has decreased significantly, from 11 % to just 3.5 %.

Table 1. Accuracy (TPR) depending on the calibration approach in a four-class classification.

	Calibration method based on:	
	Common model	Model for each taxel
SVM	0.8897	0.9648
KNN	0.8586	0.9680

4.5 Future work

As mentioned throughout the article, there are multiple issues that may be addressed in further research directions:

- Data collection for different temperature points and construction of a temperature compensation model.
- Data collection can be automated to generate larger calibration datasets. These would enable training of more complex, e.g. polynomial or convolutional, taxel model.
- Adherence to regular, twice-a-year calibration intervals in real situations and environments (hospital, home care, senior house, etc.).
- Monitoring should start from the initial installation of the pressure-sensing bed.
- Set up the maintenance strategy with a focus on the reliability of the platform's main purpose.

5. CONCLUSION

In this paper we presented a calibration method based on the recent literature in the field of pressure-sensitive RSAs. The calibration apparatus uses 3-D printed matrices that are loaded using variable weights. Thus we generate a known force, which is used as the target for training of a linear taxel model.

The sensor model, the gain and offset matrices, are learned from the data using the least-squares method and the inverse taxel models are employed to calculate the pressure force using measured conductance during monitoring of human posture. A four-class posture classification process is used to quantify the importance of the proposed calibration process: The classification error decreased from 11 % to 3.5 %. This result indicates, that a calibration is vital if we aim at accurate classification of human posture.

In future work, we may apply more complex taxel models for compensation of non-linearity, temperature effects, and deconvolution of mechanical crosstalk. The calibration should be carried out according to a predefined schedule and in a real healthcare condition monitoring application. At the current juncture, such attempts were precluded by the limited amount of data. This will require a form of automated data collection platform. A possible solution may involve a robotic manipulator, which could automatically collect calibration data using defined loading sequences.

ACKNOWLEDGEMENTS

The completion of this paper was made possible by the grant No. FEKT-S-23-8451 - "Research on advanced methods and technologies in cybernetics, robotics, artificial intelligence, automation and measurement" financially supported by the Internal science fund of Brno University of Technology.

REFERENCES

Byun, J.H., Kim, K.T., Moon, H.j., Motamedi, G.K., and Cho, Y.W. (2019). The first night effect during polysomnography, and patients' estimates of sleep quality. *Psychiatry research*, 274, 27–29. doi: 10.1016/j.psychres.2019.02.011.

Bücher, T., Huber, R., Eschenbaum, C., Mertens, A., Lemmer, U., and Amrouch, H. (2022). Printed temperature sensor array for high-resolution thermal mapping. *Scientific reports*, 12(1), 14231–14231. doi:10.1038/s41598-022-18321-6.

Dzedzickis, A., Sutinys, E., Bucinskas, V., Samukaite-Bubniene, U., Jakstys, B., Ramanavicius, A., and Morkvenaite-Vilkonciene, I. (2020). Polyethylene-carbon composite (velostat®) based tactile sensor. *Polymers*, 12(12). doi:10.3390/polym12122905.

Gilanizadehdizaj, G., Aw, K.C., Stringer, J., and Bhattacharyya, D. (2022). Facile fabrication of flexible piezo-resistive pressure sensor array using reduced graphene oxide foam and silicone elastomer. *Sensors and actuators. A. Physical.*, 340, 113549. doi: 10.1016/j.sna.2022.113549.

Halaj, M., Cudy, V., and Jasinsky, T. (1998). Calibration of the tactile sensor array. In J. Volf and S. Papezova (eds.), *Proceedings of the Eighth International Symposium on Measurement and Control in Robotics (ISMCR '98)*, 341–346.

Hastie, T., Tibshirani, R., and Friedman, J. (2009). *The Elements of Statistical Learning: Data Mining, Inference, and Prediction, Second Edition*. Springer Series in Statistics. Springer New York.

Hu, Q., Tang, X., and Tang, W. (2021). A real-time patient-specific sleeping posture recognition system using pressure sensitive conductive sheet and transfer learning. *IEEE sensors journal*, 21(5), 6869–6879. doi: 10.1109/JSEN.2020.3043416.

Husák, M., Kaczmarczyk, V., Baštán, O., and Benešl, T. (2021). Application of body posture recognition algorithm in iot smart mattress. In *2021 Selected Issues of Electrical Engineering and Electronics (WZEE)*. IEEE.

Lin, X. and Seet, B.C. (2015). A linear wide-range textile pressure sensor integrally embedded in regular fabric. *IEEE Sensors Journal*, 15(10), 5384–5385. doi: 10.1109/JSEN.2015.2453214.

Liu, S., Huang, X., Fu, N., Li, C., Su, Z., and Ostadabbas, S. (2023). Simultaneously-collected multimodal lying pose dataset: Enabling in-bed human pose monitoring. *IEEE Transactions on Pattern Analysis and Machine Intelligence*, 45(1), 1106–1118. doi: 10.1109/TPAMI.2022.3155712.

Meng, H., Zhou, L., Qian, X., and Bao, G. (2023). Design and application of flexible resistive tactile sensor based on short-circuit effect. *IEEE transactions on instrumentation and measurement*, 72, Article 9501008. doi: 10.1109/TIM.2022.3225063.

Mesárošová, M. and Mihálik, O. (2023). Sparse representation for classification of posture in bed. In *Proceedings II of the 29th Conference STUDENT EEICT 2023: Selected papers*, 101–104. Brno, Czech Republic.

Mihálik, O., Sýkora, T., Husák, M., and Fiedler, P. (2022). In-bed posture classification based on sparse representation in redundant dictionaries. In *17th IFAC Conference on Programmable Devices and Embedded Systems PDES 2022*, 374–379. Sarajevo, Bosnia and Herzegovina. doi: 10.1016/j.ifacol.2022.06.062.

Müller, S., Seichter, D., and Gross, H.M. (2019). Crosstalk compensation in low-cost resistive pressure matrix sensors. In *IEEE International Conference on Mechatronics (ICM)*, 232–237. Ilmenau, Germany. doi: 10.1109/ICMECH.2019.8722925.

Nie, B., Huang, R., Yao, T., Zhang, Y., Miao, Y., Liu, C., Liu, J., and Chen, X. (2019). Textile-based wireless pressure sensor array for human-interactive sensing. *Advanced functional materials*, 29(22), Article 1808786. doi:10.1002/adfm.201808786.

Nudzikova, P. and Slanina, Z. (2016). User identification by biometric methods. In V. Stýskala, D. Kolosov, V. Snášel, T. Karakeyev, and A. Abraham (eds.), *Intelligent Systems for Computer Modelling*, 181–190. Springer International Publishing, Cham. doi: 10.1007/978-3-319-27644-1_17.

Pang, G., Deng, J., Wang, F., Zhang, J., Pang, Z., and Yang, G. (2018). Development of flexible robot skin for safe and natural human–robot collaboration. *Micromachines*, 9(11), Article 576. doi:10.3390/mi9110576.

Peters, T., Hosur, S., Kiani, M., Roundy, S., and Trolier-McKinstry, S. (2023). Insole embedded lead zirconate-titanate film force sensor array. *Sensors and actuators. A. Physical*, 350, 114097. doi:10.1016/j.sna.2022.114097.

Stéphane, M. (2009). Chapter 11 - denoising. In M. Stéphane (ed.), *A Wavelet Tour of Signal Processing (Third Edition)*, 535–610. Academic Press, Boston, third edition edition. doi:https://doi.org/10.1016/B978-0-12-374370-1.00015-X.

Wu, J.F., Liu, B.B., Wang, F., Qiu, C., Zhao, X.G., Wang, Q., and He, S.S. (2019). Fabrication and evaluation of a stretchable thermal sensing cushion with multi-arch structure. *IEEE sensors journal*, 19(15), 6421–6429. doi: 10.1109/JSEN.2019.2910877.

Xu, X., Lin, F., Wang, A., Song, C., Hu, Y., and Xu, W. (2015). On-bed sleep posture recognition based on body-earth mover's distance. In *2015 IEEE Biomedical Circuits and Systems Conference (BioCAS)*, 1–4. doi: 10.1109/BioCAS.2015.7348281.

Zhang, H., Teoh, J.C., Wu, J., Yu, L., and Lim, C.T. (2023). Dynamic zero current method to reduce measurement error in low value resistive sensor array for wearable electronics. *Sensors*, 23(3), Article 1406. doi: 10.3390/s23031406.